Mechanical properties estimation of functionally graded materials using surface waves recorded with a laser interferometer

Laiyu Lu, Mathieu Chekroun, Odile Abraham, Valerie Maupin, Géraldine Villain

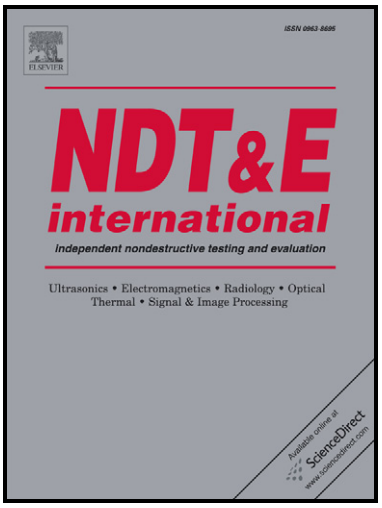

Mechanical properties estimation of functionally graded materials using surface waves recorded with a laser interferometer

Laiyu Lu, Mathieu Chekroun, Odile Abraham, Valérie Maupin, Géraldine Villain

PII: S0963-8695(10)00156-8
DOI: doi:10.1016/j.ndteint.2010.11.007
Reference: JNDT 1230

www.elsevier.com/locate/ndteint

To appear in: *NDT and E International*

Received date: 30 December 2009
Revised date: 29 October 2010
Accepted date: 17 November 2010

Cite this article as: Laiyu Lu, Mathieu Chekroun, Odile Abraham, Valérie Maupin and Géraldine Villain, Mechanical properties estimation of functionally graded materials using surface waves recorded with a laser interferometer, *NDT and E International*, doi:10.1016/j.ndteint.2010.11.007

Mechanical properties estimation of functionally graded materials using surface waves recorded with a laser interferometer

Laiyu Lu[a,b], Mathieu Chekroun[b,c], Odile Abraham[b], Valérie Maupin[d], Géraldine Villain[b]

[a] *Institute of Geophysics, China Earthquake Administration, Beijing,100081,China*
[b] *Laboratoire Central des Ponts et Chaussées, Route de Bouaye BP4129 44341 Bouguenais Cedex, Nantes,France*
[c] *Laboratoire de Caractérisation Non Destructive, Université de la Mediterrannée, 13625 Aix en Provence, France*
[d] *Department of Geosciences, University of Oslo, P.O.Box 1047,Blindern, 0316 Oslo,Norway*

Abstract

An approach is presented here to invert surface wave dispersion and attenuation relative to the depth-dependence of the visco-elastic parameters of Functionally Graded Materials (FGMs). The particularity of this method lies in allowing visco-elastic parameters to vary continuously with depth and in properly incorporating the continuous nature of these variations into both the forward problem (the calculation of dispersion and attenuation) and the inverse problem (evaluation of visco-elastic parameters). The forward problem solves the equation of elastic motion using a Runge-Kutta integration scheme, while the inverse problem is solved with the nonlinear solution for continuous inverse problems developed by Tarantola and Valette (1982). Viscoelasticity is treated as a first-order perturbation to the elastic structure. Testing on a synthetic example shows that the procedure is able to closely reproduce the S-wave velocity and attenuation profiles. As expected, the variations in P-wave velocity are not resolved, yet they do not introduce any significant bias into the S-wave velocity profile. The Rayleigh wave phase velocity and attenuation, measured by laser ultrasonic experiments, are used to infer the depth-dependence of S-wave velocity and of attenuation on mortar samples. This depth-dependence compares well with the depth-dependence derived from the sample density inferred from gamma-densitometry.

Key words: Surface waves, FGM, Inversion, Mortar

PACS: 43.20.Hq, 43.35.Cg, 43.35.Zc

1. INTRODUCTION

The interest in non-homogeneous material systems with gradually varying properties, often referred to as Functionally Graded Materials (FGMs), has recently received considerable attention in several fields of research[1–4]. As opposed to the abrupt changes encountered in media with piecewise homogeneous layers, the gradual variation in FGM material properties is known to improve failure performance while preserving the intended thermal, tribological and/or structural benefits from combining dissimilar materials[3]. Since certain performance requirements cannot be practically met with spatially uniform or multi-layered material compositions, FGMs have been enjoying widespread use in the fields of aeronautics, astronautics, etc[3, 4].

Another material that can be considered as an FGM is concrete. Concrete is characterized by its extremely heterogeneous nature since, as a common construction material, its composition includes cement or asphalt along with other materials, such as aggregates and water. The potential for a non-destructive evaluation of concrete is of major importance in monitoring the durability of civil engineering structures, especially as regards cover concrete, which is directly exposed to aggressive attack from external sources. Ultrasonic waves are often introduced to characterize such material properties; experiments have shown that wave dispersion and damping are influenced by both grain size variation and the water-to-cement ratio[5–7]. It is difficult however to generate a quantitative estimation for these properties based on measured ultrasonic signals, especially for attenuation. The main reason behind this constraint is the multiple-scattering of waves within such a heterogeneous medium, as a result of the random distribution of pores, air bubbles and aggregates when the wavelength has the same order of magnitude as the dimension of heterogeneities. The general conventional method, i.e. homogenization, has been widely employed to estimate equivalent or effective material properties[8]. Even though such estimations provide a reasonable overall prediction of mechanical behavior, they are still insufficient to accurately predict local behavior, as experiments on damaged concrete have also revealed[9, 10]. The modulus of elasticity for pavement, composed mainly of bituminous concrete, is not constant and in fact varies with depth due to a number of factors including aging, moisture content and

temperature[10, 11].

Given the growing interest in FGMs, the need for non-destructive techniques to measure their mechanical properties has become more acute. Shear-wave (S-wave) velocity and attenuation are usually considered key parameters for characterizing the mechanical properties of materials. As a non-invasive method, surface wave analysis has proven efficient in evaluating these parameters; it has been extensively used in many fields at various scales, ranging from earth imaging in geophysics[12–16] to the exploration of pavement structures in geotechnical engineering[17], as well as the estimation of material elastic properties in ultrasonic NDT (Non-Destructive Testing)[18–20]. At most scales, and particularly at the geotechnical scale[21, 22], an analysis of velocity or attenuation constitutes the main tool for extracting useful information from data. Material parameters are generally obtained by means of an inversion technique, which yields an optimal model minimizing the difference between the predicted and measured dispersion (and/or attenuation) curves of surface waves. In the geotechnical field, this method has been successfully applied in order to infer the properties of homogeneous or multi-layered media[21], although applications with continuous variations over the depth are still lacking. On the other hand, the inversion of surface wave dispersion for a continuous profile of the Earth's mantle parameters has been frequent in seismology for many years[14–16]. Due to the typically small variations of parameters in the mantle (i.e. just a few percent), dispersion curves are inverted using linear methods. In this paper, we will demonstrate that such a method may be extended to shear-wave velocity and attenuation inversions in FGMs featuring much greater variations and contrasts. This demonstration will be conducted first with a synthetic experiment, then by application to non-destructive concrete testing.

2. THEORETICAL FORMULATION AND METHODOLOGY

2.1. Forward Problem

To calculate the predicted dispersion and attenuation for a forward model, one important step involves solving the eigenvalue problem of Rayleigh waves for the visco-elastic model. In

linear viscoelasticity, this solution can be obtained by employing the same governing equations as those found in the corresponding elastic problem with identical boundary conditions, by simply replacing real variables with corresponding complex variables. In this paper, the dual conditions of linear viscoelasticity and weak dissipation have been assumed; under such an assumption, the eigenvalue for a visco-elastic model can be derived from the eigenvalue of the pure elastic case through perturbation theory[23]. As a consequence, the software developed for elastic media can easily be modified to the visco-elastic case.

The eigenvalue problem for Rayleigh waves propagating in purely elastic, layered structures can be described by differential equations in matrix form[23], i.e.:

$$\frac{d\mathbf{f}(z)}{dz} = \mathbf{A}\mathbf{f}(z) \tag{1}$$

where z is the depth coordinate, and $\mathbf{A}$ a 4×4 matrix associated with the propagator matrix, which is a function of the depth-varying compressional wave velocity V_p, shear-wave velocity V_s and density ρ . $\mathbf{f(z)}$ is a column vector that comprises the displacement vector r_1, r_2 and two elements r_3, r_4 of the stress tensor. Combined with boundary conditions, the precondition for existence of a solution to Eq.(1) yields the eigenequation of Rayleigh waves, which offers the following general form:

$$f(c_0, \omega; V_p, V_s, \rho) = 0 \tag{2}$$

where c_0 is the phase velocity of Rayleigh waves, and ω the angular frequency. The subscript 0 in this context denotes the elastic case. Both analytical and numerical methods have been developed to treat seismic wave propagation in FGMs[1, 2]. A general treatment is based on the transfer matrix approach, according to which the medium with continuously-varying inhomogeneity is regarded as a stack of many thin, piecewise homogeneous layers[23]. An explicit formulation of the transfer matrix for layered media can then be obtained. Another approach to calculating the transfer matrix of FGMs is based on an exact solution in the form of the Peano series of multiple integrals[24, 25]. In this manner, continuous inhomogeneity serves to replace the exponential solution to the wave equation by the Peano integral expression. We adopted a Runge-Kutta scheme herein to numerically integrate the

system of differential equations, derive the propagator matrices, and calculate dispersion and attenuation[23, 26].

After solving for eigenvalues, specifically the phase velocity for each frequency, the partial derivatives of phase velocity with respect to model parameters can then be obtained from the eigenfunctions by employing the variational principle[23]. The derivatives with respect to the three parameters ρ, V_p and V_s are given by the following expressions:

$$\frac{\partial c_0}{\partial \rho} = \frac{1}{2\rho}\left(\frac{\partial c_0}{\partial V_s}V_s + \frac{\partial c_0}{\partial V_p}V_p\right) - \frac{1}{2k^2UI}\omega^2(r_1^2 + r_2^2) \tag{3}$$

$$\frac{\partial c_0}{\partial V_p} = \frac{\rho V_p}{2k^2UI}\left(kr_1 + \frac{dr_2}{dz}\right)^2 \tag{4}$$

$$\frac{\partial c_0}{\partial V_s} = \frac{\rho V_s}{2k^2UI}\left[\left(kr_2 - \frac{dr_1}{dz}\right)^2 - 4kr_1\frac{dr_2}{dz}\right] \tag{5}$$

where U and k are the group velocity and wave number, respectively. I is the energy integration of the Rayleigh wave and equals:

$$I = \int_0^\infty \rho\left(r_1^2 + r_2^2\right) dz \tag{6}$$

In this paper, the software package developed by Saito has been used to calculate the Rayleigh wave eigenvalues and partial derivatives of phase velocity for the isotropic elastic model[27].

For a visco-elastic material, the modulus M^* and, by extension, both the body wave and surface wave velocities can be represented by complex quantities:

$$M^*(\omega) = M_1(\omega) + iM_2(\omega) \tag{7}$$

The degree of dissipation is often characterized by the quality factor Q, which can be expressed as:

$$Q = \frac{M_1}{M_2} \tag{8}$$

The complex modulus and velocities depend on frequency ω since the relationship between stress and strain depends on time, as a result of visco-elasticity. In addition, the

real and imaginary parts of the modulus are not independent. The relationship known as Kramers-Kronig dispersions[28], which states that visco-elastic materials are inherently dispersive, must be satisfied. In mathematical terms, this implies that M1 and M2 are Hilbert transform pairs, and this relationship constitutes the necessary and sufficient condition for M to satisfy the fundamental principle of causality[28].

Laboratory experiments show that over a broad bandwidth($10^{-2} - 10^{7}$Hz), Q can be considered as independent of frequency at very low strain levels[29]. One commonly used form of the dispersion relation that is able to satisfy the Kramers-Kronig relationship with Q remaining nearly constant is the one developed by Liu et al.[30], which can be written as [23, 31]:

$$\frac{V(\omega)}{V(\omega_{ref})} \simeq 1 + \frac{1}{\pi Q} \ln \frac{\omega}{\omega_{ref}} \tag{9}$$

where ω_{ref} denotes a reference circular frequency and V the real part of the P-wave or S-wave velocity. The dispersion relation is only applicable for weakly dissipative media, e.g. $Q > 10$, in which the dispersion caused by intrinsic dissipation remains small. Frequency-dependent modifications to the velocities introduced by attenuation are then mapped onto Rayleigh wave phase velocity variations, yielding a first-order expression using the variational principle:

$$c = c_0 + \frac{1}{\pi} \ln \left(\frac{\omega}{\omega_{ref}} \right) \int \left(\frac{\partial c_0}{\partial V_s} V_s Q_s^{-1} + \frac{\partial c_0}{\partial V_p} V_p Q_p^{-1} \right) dz \tag{10}$$

where c_0 is the phase velocity in the corresponding purely elastic model. It would appear from this expression that phase velocity dependence on the quality factor of P- or S-waves is:

$$\frac{\partial c}{\partial Q_t^{-1}} = \frac{1}{\pi} \ln \left(\frac{\omega}{\omega_{ref}} \right) \frac{\partial c_0}{\partial V_t} V_t \tag{11}$$

where the subscript $t = P, S$ denotes the compressional or shear wave, respectively.

The spatial damping of Rayleigh waves can be characterized by the dissipation factor Q_R^{-1}. For a plane Rayleigh wave propagating with an attenuation coefficient of α :

$$u = u_0 e^{-\alpha r} e^{-ikr} \tag{12}$$

Q_R^{-1} is related to α by

$$Q_R^{-1} = \frac{\alpha c}{\pi f} \tag{13}$$

Q_R^{-1} can be obtained by measuring and processing the Rayleigh wave amplitude at various distances. Q_R^{-1} depends, at the first order in attenuation, on the variations in quality factors with respect to depth via the following relation:

$$Q_R^{-1} = \frac{1}{c_0} \int \left(\frac{\partial c_0}{\partial V_s} V_s Q_s^{-1} + \frac{\partial c_0}{\partial V_p} V_p Q_p^{-1} \right) dz \tag{14}$$

This expression yields the partial derivatives of Rayleigh wave dissipation with respect to the quality factors:

$$\frac{\partial Q_R^{-1}}{\partial Q_t^{-1}} = \frac{1}{c_0} \frac{\partial c_0}{\partial V_t} V_t \tag{15}$$

2.2. Inverse Problem

For our problem, the relation between data and depth-dependent parameters can be summarized as:

$$\left[Q_R^{-1}(f), c(f) \right] = g(V_p, V_s, \rho, Q_s^{-1}, Q_p^{-1}) \tag{16}$$

where $Q_R^{-1}(f)$ and $c(f)$ are respectively the dissipation factor and phase velocity of the Rayleigh wave at each frequency f. First-order variations in the data compared to variations in model parameters are given in Equations 3, 5, 11 and 15. The inversion step consists of identifying the model or class of models that predicts measured data as closely as possible.

In this paper, the generalized nonlinear inversion technique for continuous problems, as developed by Tarantola and Valette [32], has been used to invert both the velocity and attenuation profiles. This method was designed to minimize the square of the differences between predicted and observed data on dispersion and/or attenuation.

In expressing Eq. (16) in the general form:

$$\mathbf{d} = \mathbf{g}(\mathbf{p}) \tag{17}$$

where $\mathbf{d}$ and $\mathbf{p}$ are the data and parameter sets respectively, then the inverted model at iteration $k+1$ will be given according to the least square solution for discrete nonlinear inverse problems (as proposed by Tarantola and Valette [32]) by:

$$\mathbf{p}_{k+1} = \mathbf{p}_0 + C_{p0} \cdot G_k^T \cdot (C_{d0} + G_k \cdot C_{p0} \cdot G_k^T)^{-1} \cdot \{ \mathbf{d}_0 - \mathbf{g}(\mathbf{p}_k) + G_k \cdot (\mathbf{p}_k - \mathbf{p}_0) \} \tag{18}$$

where G is the matrix of partial derivatives with respect to the model parameters, i.e.:

$$G^{i\alpha} = \partial g^i / \partial p^\alpha \tag{19}$$

For the problem treated herein, which can be calculated from the formulation described in Section 2.1, G^T is the transpose of matrix G, p_0 the *a priori* model, d_0 the data vector, $g(p_k)$ the data predicted from the model p_k, C_{p0} and C_{d0} are the *a priori* covariance matrices of the parameter and data, respectively.

The equivalent to Eq. (18) for problems with continuous variations in model parameters is expressed by:

$$\begin{aligned} p_{k+1}(z) = p_0(z) + \int dz_i \sum_i \sum_j C_{p_0}(z,z') \cdot G_k^i(z') \cdot (S^{-1})^{ij} \\ \cdot \left\{ d_0^j - g^j(\mathbf{p}_k) + \int dz'' \cdot G_k^j(z'') \cdot [p_k(z) - p_0(z)] \right\} \end{aligned} \tag{20}$$

where the matrix S_k is given by

$$S_k^{ij} = (C_{d0})^{ij} + \int dz' \int dz'' G_k^i(z') \cdot C_{p0}(z,z') \cdot G_k^j(z'') \tag{21}$$

Theoretically speaking, for a property that varies continuously with depth, we need to perform an inversion for the property at an "infinite" number of depth points in the model. In practice however, we are obviously required to sample the functions at a finite number of depth points, yet we are also intent on maintaining inversion as independent of sampling, which means introducing certain *a priori* information to constrain the inversion process. As undertaken in Leveque et al. (1991) [14], Maupin and Cara (1992) [15] and Debayle and Sambridge (2004) [33], we introduced the Gaussian-shaped function as the *a priori* covariance function of the *a priori* model p_0:

$$C_{p0}(z,z') = \sigma(z)\sigma(z') \exp\left(\frac{-(z-z')^2}{2L^2}\right) \tag{22}$$

where z and z' are two depth points, L the correlation length and σ the variance at depth z. This set-up acts as a spatial filter to smooth the model, thereby imposing a correlation between points separated by a distance on the order of L, with $\sigma(z)$ controlling the amplitude of allowable model perturbation at z. Since this approach insures that the inversion result

remains independent of discretization with depth, it is no longer necessary to sample the model with equal spacing, but rather the spacing should be greater than the correlation length.

If more than one parameter requires inversion (e.g. in this case, the shear-wave velocity V_s and P-wave velocity V_p), albeit with a certain relationship between the two being expected (perhaps through an expected Poisson's ratio), then the covariance matrix can be used to impose a correlation between the variations of the two parameters:

$$C_{p0}[Vs(z), Vp(z')] = \sigma_{V_s}(z)\sigma_{V_p}(z') \exp(\frac{-(z-z')^2}{2L^2})C_{sp} \tag{23}$$

where C_{sp} is the coupling coefficient between parameters V_s and V_p, which is capable of varying between 1 and -1. The respective variation for each parameter is controlled by its standard deviation.

In the applications that follow, we will only invert for V_s, Q_s^{-1} and/or V_p. Our software can also simultaneously invert for ρ or Q_p^{-1}, with V_s, V_p and Q_s^{-1}, although tradeoffs must be introduced whenever too many parameters are involved in the inversion process. Since Rayleigh waves are less sensitive to ρ and Q_p^{-1}, their variations are assumed to be negligible during an inversion.

3. SYNTHETIC EXPERIMENTS

The synthetic model shown in Figure 1 will be discussed in this section. We will begin by calculating the velocity and attenuation of the Rayleigh wave propagating in this model. Velocity and attenuation will then be adopted as the 'measured' data used for model property inversions. Since the model is known, it proves helpful to validate the algorithm and investigate the effects of input parameters on inversion results, such as initial model and correlation length. As is customary in the seismological literature , Q^{-1} , i.e. the inverse of quality factor Q, will be used to characterize the material attenuation.

The V_s and Q_s^{-1} profiles of this model are defined by Eq.(24) below:

$$\begin{cases} \phi(z) = \phi(d)\left\{1 + \frac{1}{2}\frac{\phi(0)-\phi(d)}{\phi(d)}\left[\frac{\tanh[a(1-2z/d)]}{\tanh a} + 1\right]\right\} & 0 \le z \le d \\ \phi(z) = \phi(d) & z > d \end{cases} \tag{24}$$

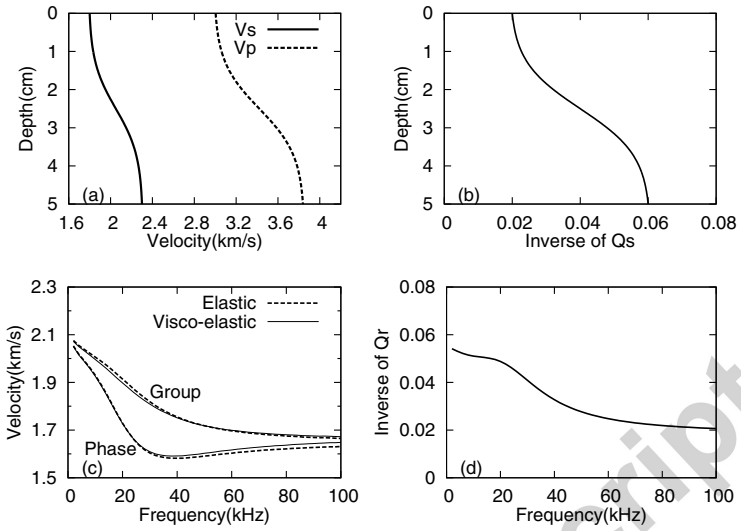

Figure 1: a) velocity profiles; b) profile of the inverse of quality factor Q_s; c) phase and group velocity of the Rayleigh wave propagating in this model; and d) inverse of the Rayleigh wave Q-value

where z is the depth. The Poisson's ratio equals 0.22 and V_p is obtained by:

$$V_p = \sqrt{\frac{2(1-\sigma)}{1-2\sigma}} V_s \tag{25}$$

Next, let $a = 2$, $d = 5$ in Eq.(24), with the model being assumed homogeneous below $5cm$. Baron et al. (2007)[24] adopted the function in Eq.(24) in order to model a transition layer, in which material properties vary continuously without any abrupt change at the edge points. These authors also discussed the forward problem for the elastic case by introducing the Peano series and went on to offer an analytical expression of the dispersion relation. This model has been extended here to the visco-elastic case in order to investigate the inverse problem. We set $V_s(0) = 1.8km/s$, $V_s(d) = 2.3km/s$. It is assumed that Q_s^{-1} exhibits the same variation as V_s and that $Q_s^{-1}(0) = 0.02$, $Q_s^{-1}(d) = 0.06$. Q_p^{-1} is also assumed to satisfy the equation in[34], i.e.:

$$Q_p^{-1}(z) = \frac{4}{3}\frac{V_s^2(z)}{V_P^2(z)} Q_s^{-1}(z) \tag{26}$$

Figures 1a and b show the velocity and Q_s^{-1} profiles of this model, while Figures 1c and d indicate the velocity and Q^{-1} of the Rayleigh wave. The velocity for the pure elastic case is

also given in Figure 1c.

In civil engineering, the Poisson's ratio, instead of the V_p profile, of materials can sometimes be approximately estimated as *a priori* information. Figure 2 displays the inversion results with a known Poisson's ratio (0.22) as the *a priori* information. The initial model, inverted profiles and true model are all presented in this figure. The initial value of V_s consists of the profile $1.1c - 0.5\lambda$. In early geotechnical engineering practice, this profile was often used to approximate the V_s profile. The two coefficients (1.1 and 0.5) may at times be modified depending on the expected Poisson's ratio of the medium. We performed a large number of calculations for various initial models, and this profile proves to be a better initial model than a constant profile. The initial values of Q_s^{-1} can be chosen depending on the Q^{-1} of Rayleigh waves. A morderate value for Rayleigh wave Q^{-1} turns out to be a good initial model for Q_s^{-1}. The initial V_p is generated from V_s by means of a known Poisson's ratio. Figure 2 reveals a set of good inversion results obtained for Q_s^{-1}, V_s and hence V_p.

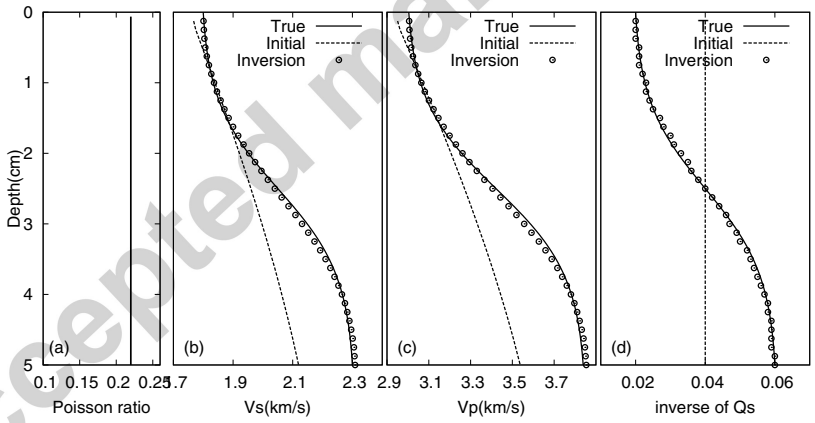

Figure 2: Inversion results with a known Poisson's ratio. (a),(b),(c) and (d) are the profiles of Poisson's ratio, S-wave velocity, P-wave velocity and Q^{-1}, respectively.

In contrast, without any *a priori* information on the Poisson's ratio and V_p, inverting for V_s and V_p as the independent parameters may be preferred. Figure 3 presents the inversion results for this particular case. Compared to Figure 2, Figure 3 shows that larger differences between the true and inverted velocity profiles are observed within the $4cm - 5cm$ range for

V_s and Q_s^{-1}. This case features less *a priori* information and a higher number of inverted parameters, which in turn increases the level of inversion uncertainty. For P-wave velocity V_p, the difference between the inverted and true models is considerable. As a consequence of the low sensitivity of Rayleigh waves to V_p, the inverted V_p profile has in fact changed very little compared to the initial model. Even though the inverted V_p is far from the true model, the inverted phase velocity and Q^{-1} of the Rayleigh wave display good agreement with the data, which implies that the inverted V_p is not reliable and moreover that the same dispersion curves and Q^{-1} can allow for multiple solutions of V_p. Numerical results for the other synthetic test also support this finding. In a practical application therefore, we should seek *a priori* information on the Poisson's ratio or P-wave velocity of the materials using the other method, such as reflection and refraction method. It should be pointed out however that the incorrect V_p profile does not significantly bias the inverted V_s and Q_s^{-1} profiles and that these profiles can be properly recovered even in the absence of accurate knowledge on V_p or Poisson's ratio.

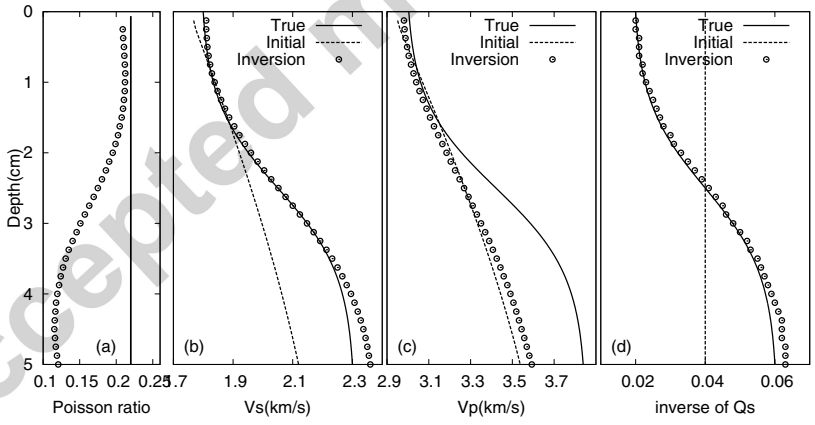

Figure 3: Identical to Fig.2, yet without knowing the value of Poisson's ratio.

4. APPLICATION: DETERMINATION OF MORTAR PROPERTIES FROM LASER MEASUREMENTS

In this section, the method described above will be applied to perform an inversion for the shear-wave velocity (correspondingly the Poisson's ratio) and for the attenuation of a mortar sample, based on surface wave data collected using a laser interferometer.

4.1. Experimental set-up and measurements

Experimental measurements have been carried out on mortar samples with a maximum grain size of $D_{max.} = 4\,mm$. Two series of mortar slabs M1 and M2, differing in just their water/cement ratio, were considered: the M1 series has a low water/cement ratio ($w/c = 0.35$), while the M2 ratio is higher ($w/c = 0.65$), thus inducing higher porosity. CEM 1 52.5N CE CP2 NF cement has been used and the granulate are silico calcareous. The slabs were held underwater in between experiments to ensure remaining fully saturated at all times. Each series was composed of 5 identical slabs with dimensions $600\,mm \times 600\,mm \times 120\,mm$. The $120\,mm$ specimen thickness was considered sufficient to ensure that signals received at the surface corresponded to Rayleigh waves, thus avoiding the generation of Lamb wave modes.

A piezoelectric transducer equipped with a wedge was used as a source to generate Rayleigh waves in the mortar slabs. The source function was a Ricker wavelet with a central frequency equal to 120 kHz. Reception was performed with a laser interferometer (*Tempo from Bossa Nova Tech*), which acquires the normal displacement at the slab surface according to a non-contact protocol. The laser beam position was controlled by a robot to allow for an acquisition every $1\,cm$ at a distance from the source ranging from $10\,cm$ to $45\,cm$, to yield the equivalent of a common-shot gathers in seismology. The precision of the laser beam position is better than $0.01mm$ and the data acquisition card has a sampling rate equal to $10MHz$ and a 16 bits resolution[35].

To take into account the heterogeneous nature of the mortar (i.e. size and position of sand, presence of bubbles and other surface inhomogeneities[36]), a total of 36 similar common-shot gathers were collected at different positions on the 5 slabs for each series; a

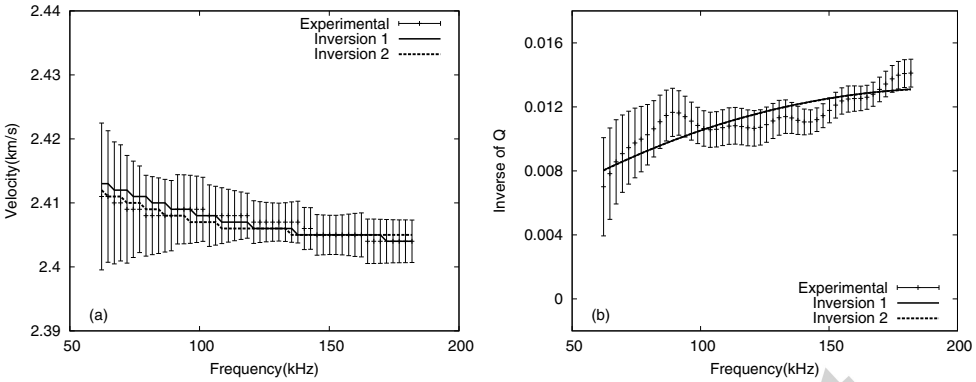

Figure 4: Rayleigh wave phase velocity (a) and Q^{-1} (b) of both the experimental and inverted models for mortar M1

spatial average could then be established to obtain the coherent field.

Geometrical spreading was corrected from the measurements by multiplying all signals by $\sqrt{r}$, where r is the distance from the source. We used a $p-\omega$ transform to extract the phase velocity dispersion curves[37], where p represents the slowness of the waves ($p = 1/c$) and ω the angular frequency. This method transform the multi-channel data wave field into the slowness-frequency domain. In $p-\omega$ domain, the maximum will be reached at the eigenvalues of the Rayleigh wave. The algorithm proposed by Herrmann is used to extract the velocities for each frequency and also provides error bars[38]. The attenuation factor is estimated from the decrease of the amplitude spectrum of the coherent field during propagation. Damping factor vs. frequency was evaluated by performing a linear fit of the natural logarithm of the spectral amplitude[39].

Figure 4 provides the experimental phase velocity and error bars. Due to limitation in the transducer frequency band as well as the signal-to-noise ratio, only data in the 60-180 kHz bandwidth could be introduced. This frequency range corresponds to wavelengths ranging from approximately 10mm to 40mm[36]. The spectrum modulus of the Rayleigh waves at this bandwidth is larger than -20dB. The interval between two adjacent frequencies is 2440Hz. Details about the experiment and extraction of the dispersion curves can be found in reference[39].

Dispersion of Rayleigh waves may arise from two phenomena: the variation with depth of the properties of the media and the dispersion of P and S waves related to multiple scattering in heterogeneous media. The scattering produces in addition attenuation. It is therefore in theory possible to distinguish between the two effects by a combined analysis of dispersion and attenuation. However, the frequency range used here corresponds to wavelength varying from 10 to 40 mm, while in the mortar series M1 and M2 the maximum grain size is $D_{max} = 4\,mm$. Then the wavelength is much bigger than the heterogeneities of mortar, inducing negligible scattering effects. The scattering-related dispersion of P and S waves in the mortars used here and in associated concrete samples has been studied in reference[36]. They find that for the concrete samples, which in essence contain bigger heterogeneities (coarse aggregates of $D_{max} = 20\,mm$) than the mortar samples, scattering related to heterogeneities generates a noticeable additional dispersion compared to the mortars, in the actual frequency range. In addition, the scattering by aggregates produces an attenuation about three times the one observed for mortars. We conclude that for the mortar used here, the major part of the dispersion is likely to originate from depth-dependence of the structure.

4.2. Inversion results

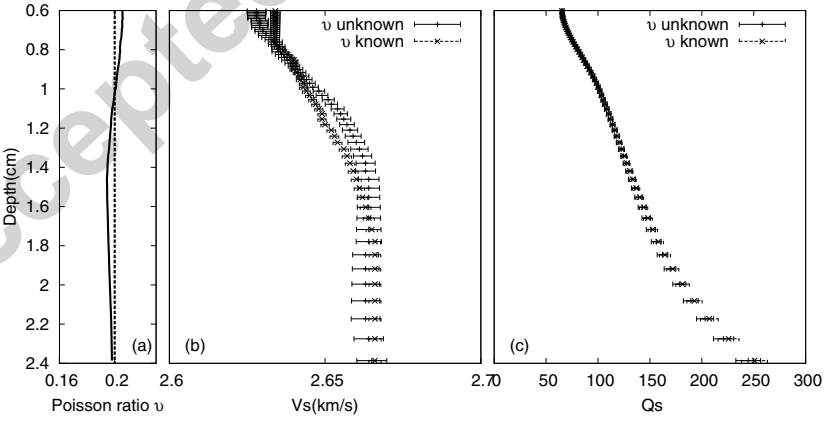

Figure 5: Inversion results for mortar M1 - two results are shown, one with an unknown Poisson's ratio and the other with a known estimated Poisson's ratio equal to 0.2

Figure 5 shows the inversion results for the M1 series. The correlation length has been

set at $0.5cm$, and the *a priori* variance is $0.002km/s$ for V_s and V_p and 2×10^{-4} for Q^{-1}. In comparison with synthetic models, a greater number of iterations was required here before obtaining convergence. We conducted a total of 100 iterations and typically reached convergence after between the 50th and 60th iteration. In order to compare results for different *a priori* information, the inversion procedure was carried out in two ways: first with an unknown Poisson's ratio ν, where V_s, V_p and Q_s were inverted simultaneously; and second with a known Poisson's ratio given as *a priori* information, where only V_s and Q_s were inverted. No real significant differences are observed in Figure 5, except for the larger a posteriori error obtained on the inversion with an unknown Poisson's ratio. This finding is not difficult to explain since the constraint imposed on the inversion procedure without an a priori Poisson's ratio was less stringent. Similar trends and orders of magnitude were observed for these series of results. Figure 4 indicates that these two inverted dispersion and Q^{-1} curves fit the experimental data quite well. Based on this example and in recalling the discussion on numerical models in the previous section, it is considered an appropriate choice to perform the inversion with an *a priori* Poisson's ratio estimated from experience.

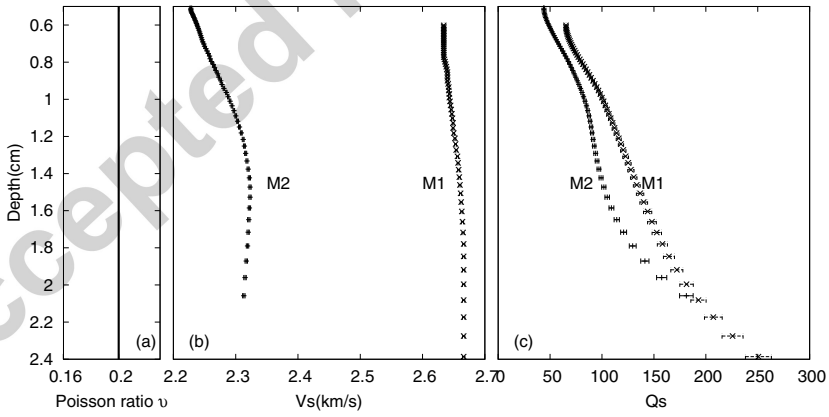

Figure 6: Inversion results for mortars M1 and M2.

Figure 6 presents the inversion results for M2 and M1, with a known and constant Poisson's ratio set equal to 0.2. As expected, it was observed that the shear-wave velocity of mortar M1 exceeded that of mortar M2, since M2 is more porous. Similarly, the quality

265 factor Q_s of M1 was greater than that of M2 at all depths. For both mortars, a slight
266 dispersion in the phase velocity dispersion curve is visible, hence indicating that material
267 properties vary with depth. At low frequencies, phase velocity increases such that a higher
268 body-wave shear velocity with depth can be expected. This observation is in accordance
269 with common knowledge held on concrete properties. The first few millimeters contain
270 fewer aggregates than lower depths due to a wall effect: the proportion of large aggregates
271 becomes constant after a depth equal to the radius of the largest aggregate[40]. To be
272 able to explain this increase of wave velocity, we performed density profile measurements by
273 gammadensitometry[41]. In the slabs the density is increasing towards the surface(See Figure
274 8 for the density variation). We suppose that this phenomenon is due to the use of a wood
275 form that is coated with bakelite so that bleeding water is not absorbed by this formwork on
276 the contrary to wooden formwork classically used for concrete structures. As a consequence,
277 this higher quantity of water available near the surface, during setting, is increasing density
278 by chemical reaction in this area compared to the depth. Furthermore, the grain size is
279 surely modifying the density near the surface, and this phenomenon is competing with pore
280 size and pore distribution near the surface together with water gradient that can extend to
281 different depth[41].

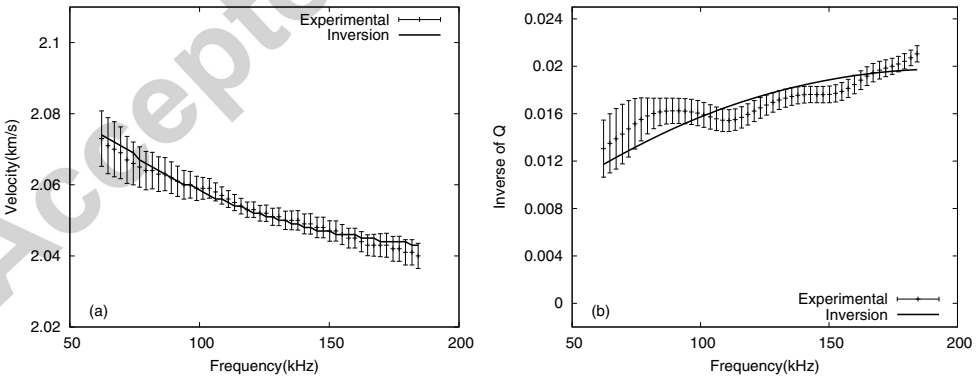

Figure 7: Rayleigh wave phase velocity (a) and Q^{-1} (b) of both the experimental and inverted models for mortar M2

282 For the inversion step, a constant Poisson's ratio of 0.2, i.e. a classical value for mortar,

283 was chosen. It is apparent on the shear-wave velocity profiles that below 1.5 cm, the mortar
284 can be considered homogeneous with a shear-wave velocity equal to 2,660 $\mathrm{m.s^{-1}}$ for M1 and
285 2,330 $\mathrm{m.s^{-1}}$ for M2. Figure 7 shows the experimental phase velocity and attenuation with
286 error bars, together with the corresponding inverted one.

287 The depth limits for the two inverted profiles are slightly different because the higher
288 phase velocity in M1 yields slightly larger wavelengths, and therefore larger penetration
289 depths, than in M2, for the same frequency range. The inverted V_s profiles for M1 and
290 M2 tend to display a typical characteristic, namely increasing smoothly with depth over the
291 first few millimeters near the surface, with an inflection point observed at $1.4 - 1.6cm$, then
292 tending to a constant value at greater depths. This finding is a result of aggregate size,
293 the presence of air bubbles and a saturation rate capable of differing nearer the surface and
294 deeper due to the wall effect and exposure to air. Consequently, the density may feature
295 similar characteristics. To verify these inverted profiles, we measured the mortar sample
296 density at various depths using gamma-densitometry. It should be pointed out this does
297 not mean we attribute the velocity variation only to the density variation. The shear wave
298 velocity variation is related to several parameters such as density, Young's modulus and
299 water content, often in competition.

Figure 8 shows the density profiles with errors measured by means of gamma-densitometry for mortars M1 and M2; average density equals 2,256±5 kg/m^3 for M1 and 2,151±17kg/m^3 for M2. A difference in density is noticed near the edges, as a result of the skin effect. For the sake of comparison, we used the function with exponential attenuation to fit measurements (counting from the surface):

$$f = f_0 + Ce^{-x/a} \tag{27}$$

300 where f and x denote density and depth, respectively. C and a are the constants to
301 be determined. The function and its graph are shown in Figure 8. For M1, the profile is
302 nearly symmetrical on both sides. At a depth of 1.5-2.0cm from the surface (as denoted by
303 two circles drawn in a dashed line), a similar inflection point can be observed. The density
304 tends to a constant between the two inflection points. The profile shape and inflection point
305 location closely match the V_s profile. For M2, the density profile is not symmetrical from

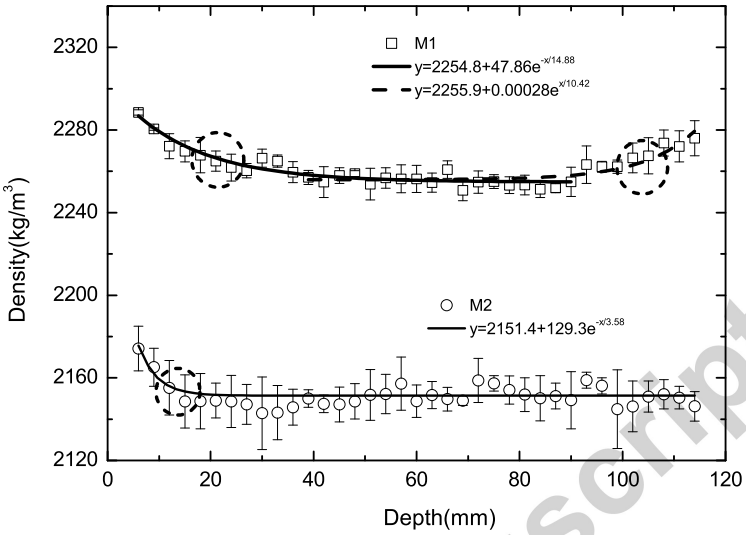

Figure 8: The density profiles for M1 and M2 measured by gamma-densitometry.

both sides of the surface. This outcome is likely due to the presence of air bubbles near one side (where depth equals 120mm on Fig.8). Air bubbles are usually removed by hammer blows for different samples on both sides of all slabs. For mortar M2 however, the protocol perhaps differed on the side of the slab used for gamma-densitometry coring samples, which could explain the difference in density near the 120mm deep side. For mortar M2 near the other side (i.e. 0mm depth), the same density variations as for mortar M1 can be observed, which is why density measurements have, to some extent, confirmed our inverted Vs profile and thereby offer a reliable verification for our method.

5. DISCUSSION AND CONCLUSION

We have presented herein a method for inverting surface wave dispersion and attenuation in terms of the depth-dependent visco-elastic parameters of Functionally Graded Materials (FGMs). The particularity of this method lies in the fact that the visco-elastic parameters are allowed to vary continuously with depth and that both the forward problem (involving

calculation of dispersion and attenuation) and the inverse problem (evaluation of visco-elastic parameters) effectively take into account the continuous nature of these variations. The forward problem solves the equation of elastic motion using a Runge-Kutta integration scheme. The viscous part is treated as a first-order perturbation to the elastic structure, which limits method applicability to materials with weak attenuation.

The inverse problem is treated using the nonlinear solution to continuous inverse problems developed by Tarantola and Valette (1982)[32]. This set-up allows for continuous variations, without having to define a set of functions over which the profile is to be decomposed. The inversion step is dependent on a prescribed correlation length for the particular profile and not on its sampling with depth. This protocol is very flexible and enables representing a large set of models very easily. Our software introduces interfaces at prescribed depths, yet this option has not been adopted in the present application. The starting model is defined by a simple formula directly related to the dispersion curve. Problem non-linearity is taken into consideration by iterating linear inversions; we have shown that convergence towards the correct profile is obtained after just a few iterations in the purely elastic case, but a larger number of iterations is required in the case of attenuation.

Dispersion and attenuation have been inverted simultaneously for the S-wave velocity, attenuation and, in some cases, for P-wave velocity. The dispersion due to attenuation has also been incorporated, thus avoiding erroneous mapping as a result of depth-dependent, S-wave velocities. P-wave velocity variations can also be accounted for either by including them as a parameter to be inverted or by coupling their variations to those of the S-wave velocity through a fixed Poisson's ratio value. Partial coupling via a correlation coefficient between 0 and 1 is also possible.

The Rayleigh wave phase velocity and attenuation measured by means of laser ultrasonic experiments are used to infer the depth-dependence of S-wave velocity and attenuation on mortar samples. It has been found that mortar inhomogeneity is confined to the first $1.5cm$ of depth. This depth-dependence compares well with that of the sample density inferred from gamma-densitometry.

The procedure implemented has been designed to analyze the variations in elastic param-

eters with depth; moreover, we assumed herein that the material is homogeneous in the two horizontal directions. This method however may still be combined with other techniques in order to recover the depth-dependence and lateral variations of the elastic parameters. In the case of randomly distributed lateral heterogeneities, such as those in the mortar samples, stacking several recordings has yielded information on the average structure. In the case of lateral variations that are consistent with respect to the length of analyzed surface waves, it can be shown that the dispersion measured between two points depends on the average structure between points[42]. Average structures along many paths can then be interpreted within a 3-D structure using various tomographic techniques[12–16, 33, 43]. As an alternative, local measurements of dispersion and their inversion with depth can serve to map lateral variations more directly[44].

Finally the possibility of using surface wave to investigate variation of properties of the first centimeter of concrete (cover concrete) are underway. A major step will consist in dealing with the strong scattering on our measurements as the wavelength will be of the same order of grandeur as the aggregates (few centimeters).

ACKNOWLEDGMENTS

The authors would like to thank the Electricit de France (EDF) utility company for financing a portion of the research. This work effort was also partially supported by the European INTEREG IIB program MEDACHS and the French ANR project SENSO, as well as by the National Natural Science Foundation of China (40974032).

References

References

[1] W.Q. Chen, H.M. Wang and R.H. Bao, On calculating dispersion curves of waves in functionally graded elastic plate, *Composite structures*, **81**,233-242(2007)

[2] K. Baganas, Wave propagation and profile reconstruction in inhomogeneous elastic media, *Wave Motion*, **42**,261-273(2005)

374 [3] A. Carpinteri and N. Pugno, Cracks and re-entrant corners in functionally graded ma-
375 terials, *Engineering Fracture Mechanics*, **73**,1279-1291(2006)

376 [4] F. Erdogan and B.H. Wu, Fracture mechanics of functionally graded materials, *Compos.*
377 *Engng.*, **7**,753-770(1995)

378 [5] T.P. Philippidis and D.G. Aggelis, Experimental study of waves dispersion and atten-
379 uation in concrete, *Ultrasonics*, **43**,584-595 (2005).

380 [6] L.J. Jacobs and J.O. Owino, Affect of Aggregate Size on Attenuation of Rayleigh Surface
381 Waves in Cement-Based Materials, *J. Eng. Mech. ASCE* **126**(11), 1124-1130 (2000)

382 [7] J.O. Owino and L.J. Jacobs, Attenuation Measurements In Cement-Based Materials
383 Using Laser Ultrasonics, *J. Eng. Mech. ASCE*, **125** (6), 637-647 (1999)

384 [8] D.G. Aggelis and S.V. Tsinopoulos and D. Polyzos, An iterative effective medium ap-
385 proximation (IEMA) for wave dispersion and attenuation predictions in particulate
386 composites, suspensions and emulsions, *J. Acoust. Soc. Am.*, **116**,3443-3452(2004).

387 [9] D.G. Aggelis and T. Shiotani, Experimental study of surface wave propagation in
388 strongly heterogeneous media, *J. Acoust. Soc. Am. Express Letters*, **122**,EL151(2007).

389 [10] E.V. Dave, W.G. Buttlar, Glaucio H. Paulino and Harry H. Hilton, Graded visco-
390 elastic approach for modeling asphalt concrete pavement, AIP Conference Proceedings,
391 **973**,736-741(2008).

392 [11] P. Ullidtz, Pavement analysis, developments in civil engineering, (Elsevier, Amestr-
393 dam,1987)

394 [12] J.H. Woodhouse and A.M. Dziewonski, Mapping the upper-mantle 3-dimensional mod-
395 eling of Earth structure by inversion of seismic waveforms, *J. Geophys. Res.*, **89**, 5953-
396 5986(1984).

397 [13] A. Curtis, R. Snieder, Probing the earth's interior with seismic tomography, in In-
398 ternational handbook of earthquake and engineering seismology, Eds. Lee, W.H.K.,

399 H. Kanamori, P.C. Jennings, and C. Kisslinger, Academic Press, Amsterdam, 861-
400 874(2002).

401 [14] J.J. Leveque, M. Cara and D. Rouland, Waveform inversion of surface wave data:test of
402 a new tool for systematic investigation of upper mantle structures, *Geophysics J. Int.*,
403 **104**,565-581(1991).

404 [15] V. Maupin and M. Cara, Love-Rayleigh wave incompatibility and possible deep upper
405 mantle anisotropy in the Iberian Peninsula, *Pure and Applied Geophysics*, **138**,429-
406 444(1992).

407 [16] A.M. Dziewondki, A.L. Hales and E.R. Lapwood,Parametrically simple Earth models
408 consistent with geophysical data, *Phys. Earth planet. Int.*, **10**, 12-48(1975).

409 [17] N. Ryden and M.J.S Lowe, Guided wave propagation in three-layer pavement structures,
J.Acoust. Soc. Am., **116**,2902-2913(2004).
410

411 [18] T.T. Wu and Y.H. Lui, Inverse determinations of thickness and elastic properties of a
412 bonding layer using laser-generated surface waves, *Ultrasonics*, **37**, 23-30(1999)

413 [19] Y.S. Cho, Non-destructive testing of high strength concrete using spectral analysis of
414 surface waves, *NDT & E Int.*, **36**,229-235(2003).

415 [20] Y.S. Cho and F.B. Lin, Spectral analysis of surface wave response of multi-layer thin
416 cement mortar slab structure with finite thickness, *NDT & E Int.*, **34**,115-122(2001).

417 [21] C.P. Park, R.D. Miller and J.H Xia, Multichannel analysis of surface waves,*Geophysics.*
418 **64**,800-808(1999).

419 [22] M. Alam, J.H. McClellan and W.R. Scott, Spectrum analysis of seismic surface waves
420 and its applications in seismic landmine detection, *J. Acoust. Soc. Am.*, **121**,1499-
421 1509(2007)

[23] K. Aki and P.G. Richards, Quantitative Seismology, (Freeman & Co., San Franciso,1980)

[24] C. Baron, A.L. Shuvalov and O. Poncelet, Impact of localized inhomogeneity on the surface-wave velocity and bulk-wave reflection in solids, *Ultrasonics*, **46**,1-12(2007)

[25] A.L. Shuvalov, O.Poncelet and M.Deschamps, General formalism for plane guided waves in transversely inhomogeneous anisotropic plates, *Wave Motion*, **40**,413-426(2004)

[26] H. Takeuchi and M. Saito, "Seismic surface waves. In seismology: surface waves and earth oscillations" in*Methods in computational physics*, edited by B. A. Bolt, (Academic Press,New York,1972), Vol. 11,pp. 217–295.

[27] M. Saito, "Disper80: a subroutine package for the calculation of seismic normal mode solutions", in *Seismological algorithms:computational methods and computer prorams*, edited by Durk J. Doornbos, (Academic Press,New York,1988),pp. 293–319.

[28] J.M. Carcione, Wave fields in real media: wave propagation in anisotropic, anelastic and porous media,(Pergamon, UK,2002)

[29] M.N. Toksoz, D.H. Johnston and A. Timur, Attenuation of seismic waves in dry and saturated rocks: I. Laboratory measurements, *Geophysics*, **44**,681-690(1979).

[30] H.P. Liu and D.L. Anderson and H. Kanamori, Velocity dispersion due to anelasticity: Implications for seismology and mantle composition, *Geophys. J. Roy. Astron. Soc.*, **47**,41-58(1976).

[31] E. Kjartansson, Constant Q-Wave propagation and attenuation, *J. Geo. Res.*, **84**,4737-4748(1979)

[32] A. Tarantola and B. Valette, Generalized nonlinear inverse problem solved using the least squares criterion, *Reviews of Geophysics and Space Physics*, **20**,219-232(1982)

[33] E. Debayle and M. Sambridge, Inversion of massive surface wave data sets:Model construction and resolution assessment, *Journal of Geophysical Research*, **109**,B02316(2004)

[34] D.L. Anderson, "Theory of the Earth",(Blackwell Scientific Publications,1989)

[35] F. Bretaudeau, D. Leparoux, O. Durand and O. Abraham, "Small-scale modeling of onshore seismic experiment: a tool to validate numerical modeling and seismic imaging methods",submitted to Geophysics (2010)

[36] M. Chekroun, Caractérisation mécanique des premiers centimètres du béton avec des ondes de surface, *Ph.d Thesis*, Ecole Doctoral SPIGA(498),Nantes, France(2008)

[37] T.A. Mokhtar, R.B. Herrmann and D.R. Russel, Seismic velocity and Q model for the shallow structure of the Arabian shield from short-period Rayleigh waves, *Geophysics*, **53**(11):1379-1387(1988).

[38] R.B. Herrmann, Computer Program in Seismology, Department of Earth and Atmospheric Science, Saint Louis University, 2002, *http://www.eas.slu.edu/People/ RBHerrmann/ComputerPrograms.html*

[39] M. Chekroun, L. Le Marrec, O. Abraham, G. Villain, O. Durand , Analysis of coherent wave dispersion and attenuation for non-destructive testing of concrete, *Ultrasonics*, doi:10.1016/j.ultras.2009.05.006(2009).

[40] J. J. Zheng, C. Q. Li, M. R. Jones. Aggregate distribution in concrete with wall effect, *Magazine of Concrete Research*, **55**(3):257-2659(2003).

[41] G. Villain and M. Thiery, Gammadensimetry: A method to determine drying and carbonation profiles in concrete, *NDT & E Int.*, **39**(4):328-337(2006).

[42] J.H. Woodhouse, Surface waves in a laterally varying layered structure, *Geophys. J. R. astro. Soc.*, **37**, 461-490(1974).

469 [43] N.M. Shapiro and M.H. Ritzwoller, 2002. Monte-Carlo inversion for a global shear
470 velocity model of the crust and upper mantle model, *Geophys. J. Int.*, **151**, 88-105.

471 [44] F.C. Lin, M.H. Ritzwoller and R. Snieder, Eikonal tomography: surface wave tomog-
472 raphy by phase front tracking across a regional broad-band seismic array, *Geophys. J.*
473 *Int.*, **177**, 1091-1110(2009).